DOI: 10.13009/EUCASS2022-6150
9TH EUROPEAN CONFERENCE FOR AERONAUTICS AND SPACE SCIENCES (EUCASS)

# Numerical Turbine Blade Fatigue Life Analysis for Reusable Liquid Rocket Engines (LREs) Applications

*Mateusz T. Gulczyński*, Robson H. S. Hahn**, Jörg R. Riccius**, Evgeny B. Zametaev**, Günther Waxenegger-Wilfing**, Jan C. Deeken**, Michael Oschwald**

**German Aerospace Research Center DLR Lampoldshausen, RWTH Aachen University, Germany*
*Mateusz.Gulczynski@dlr.de, Michael.Oschwald@dlr.de, Jan.Deeken@dlr.de*
*** German Aerospace Research Center, DLR Lampoldshausen, Germany*
*Robson.DosSantosHahn@dlr.de, Joerg.Riccius@dlr.de, Evgeny.Zametaev@dlr.de, Guenther.Waxenegger@dlr.de*

## Abstract

Nowadays reusability of LREs, represented in projects such as CALLISTO and Maïa (both including the re-usable Prometheus engine), is seen not only as essential in the effort to prepare competitive future European space access, but also sets a new requirement towards high reliability engineering standards. With engine operation life in excess of a single mission, it is necessary to evaluate the most critical components, which could develop cracks as in case of the e.g. the turbopump turbine BLISK (Blade Integrated Disk) and, as a result, lower the total engine flight life [1], [2].

Within our research we focus on the turbine blade analysis for reusable LRE applications including high cycle fatigue (HCF) and low cycle fatigue (LCF). Turbine blades are subjected to large thermo-mechanical cyclic strains arising from the high temperatures driving gas in combination with a fast start-up sequence as well as high rotational speed – crucial for obtaining high performance and structural mass efficiency for LREs [3], [4], [5].

To predict the turbine blade fatigue life, we compare an analytical (0D) and numerical (3D FE) approach for a selected test case. The fatigue life analysis evaluates the BLISK at the highest loading condition accounting for HCF by a modified Goodman approach.

**Key words:** Ariane Next, BLISK, CALLISTO, High Cycle Fatigue (HCF), Liquid Rocket Engines, LUMEN, Maïa, Prometheus, Reusable Launch Vehicle (RLV), Themis, Turbine Blade, Turbopump

## 1. Introduction

The reusability technology of future European launchers is advancing through commencing projects such as THEMIS and CALLISTO – reusable demonstrators for vertical take-off and landing (VTVL), as well as reusable rockets namely MAÏA (the new French micro launcher for payloads up to 1 ton) or Ariane Next, all powered by the reusable cryogenic Oxygen/Methane (LOX/$LCH_4$) engine "Prometheus" [6], [7]. To enable the further enhancement of reusability systems and to develop cost-effective and reliable liquid rocket engines (LREs), studies on critical engine components such as turbopumps are essential. Principally, when it comes to BLISK elements where creep-fatigue effects, thermal shock and thermal distribution arising from the admission of hot gases at full flow is expected, it is crucial to evaluate the turbine blades failure incorporating rotational, gas pressure, shrink fitted, mechanical and thermal loads. Within the presented research, the validation of several of the applied analytical and numerical methods is established through the Liquid Upper stage deMonstrator ENgine (LUMEN) which was developed at DLR Lamploldshausen to strengthen the expertise in the complete cycle operation for various engine applications, as well as to empower validation studies of operational conditions to which turbopump components, such as turbine blades, are subjected [1]. The LUMEN demonstrator is an expander bleed cycle engine, operated by the bipropellant combination liquid oxygen (LOX) and Methane. In the frame of the presented analysis, the fatigue behaviour of the Oxidizer Turbopump (OTP) BLISK is evaluated, where input operational conditions as well as dimensions of rotor, disk and blades are acquired from the LUMEN demonstrator [8].
The paper is organized in the following way: in section 2, the analytical approach towards calculating the basic loads is presented along with LUMEN's OTP characteristics. Subsequently, in section 3, the numerical analysis is shown. Finally, in the concluding section 4, a summary of the results with perspective on the following activities is specified.

DOI: 10.13009/EUCASS2022-6150



## 2. Beam Theory Structural Analysis of the LUMEN Oxidizer Turbopump (OTP)

As the turbine blade can be considered as a beam, consequently the beam theory is applied. For the given boundary conditions and based on the input values, the centrifugal and gas bending stresses are estimated – incorporating reaction and internal forces that act on the turbine blade. Such an approach is versatile, and therefore may be applied to estimate the loads in any turbine type model. In Fig. 1, the geometrical parameters along with veolcity triangles for calculating centrifugal and gas bending stresses is presented. The analytical approach is explained in the following sections.

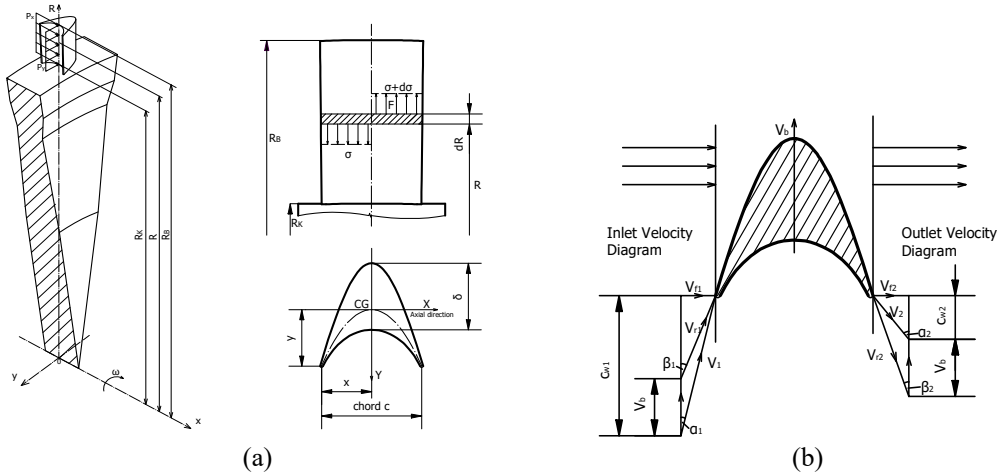


Fig. 1 Schematic of the LUMEN OTP (a) blade geometry ("$R_K$" – root radius, "$R_B$" – tip radius, "$R_{mean}$" – blade centroid radius), (b) velocity triangles in front of and behind the blade ($\alpha_1 = 74.04^o$, $\alpha_2 = 47.60^o$) (M. T. Gulczyński *et al.*)

The general turbopump design process commences with calculation of the main pump RPM established from the net positive suction pressure (NPSP), the volumetric flow rate, as well as the suction specific speed [2]. This is realized in combination with a total pump pressure rise obtained from the engine fluid circuit analysis and utilized for establishing the required total pump pressure. Based on the above-mentioned, the number of stages, diameter, pump efficiency including size with weight is determined. The analysis of the oxygen turbopump continues with calculating the turbine exit gas pressure, based on the entrance conditions acquired from the LUMEN demonstrator flow path analysis. Similarly to LUMEN's fuel turbopump, further values including U/Co (velocity ratio), rotational and specific speed, diameter, admission fraction, are subsequently calculated and utilized to compute the turbine efficiency. These values, as outlined in Table 1, are then incorporated into loads calculation and fatigue life study [1], [9], [10], [11].

Table 1 LUMEN's OTP input data

| ***Nomenclature*** | **Parameter** | **Value** | **Unit** |
|---|---|---|---|
| *Mass of the blade* | $m$ | 0.0017 | kg |
| *Radius of the blade centroid* | $R_{mean}$ | 0.0635 | m |
| *Number of blade driving jets* | $n_{stat}$ | 3 | - |
| *Rotational speed of the OTP (for BP8)* | $\omega_{OTP}$ | 2807.2 | rad/sec |
| *Cross-sectional area of the blade* | $A$ | $2.3 \cdot 10^{-5}$ | $m^2$ |
| *Stress concentration factor* | $K_t'$ | 2.5 | - |
| *Fillet radius (transition between the disk and the blade)* | $r_{fillet}$ | 0.005 | m |
| *Blade height* | $h_{OTP}$ | 0.0093 | m |
| *Number of blades* | $n_{blades}$ | 65 | - |
| *Input for the calculation of the blade camber angle* | $\beta_{1r}$ | 69 | ° |
| *Input for the calculation of the blade camber angle* | $\beta_{2r}$ | 18 | ° |
| *In accordance with the blade camber angle diagram* | $n$ | 1.27 | - |
| *In accordance with the blade camber angle diagram* | $B$ | 570 | - |
| *Maximum blade thickness* | $t_{OTP}$ | 0.00370 | m |
| *Chord length* | $c$ | 0.009 | m |
| *Tangential component of entering stream (whirl velocity)* | $C_{w1}$ | 246.9 | m/s |
| *Corresponding value at exit of the moving blade* | $C_{w2}$ | 201.9 | m/s |
| *Mass flow rate* | $\dot{m}$ | 1.046 | kg/s |
| *Admission degree of the OTP* | $\Theta_{OTP}$ | 0.229 | |

DOI: 10.13009/EUCASS2022-6150



## 2.1 Centrifugal stress

The assessment of the steady-state stresses in blades is crucial to achieve acceptable evaluation margins for omitting High Cycle Fatigue (HCF) as well as for defining a turbine creep deformation criterion. The preeminent element of the steady blade stress is the centrifugal stress, whereas gas bending, shroud and fixing, and thermal stresses are less significant [3]. The 0D centrifugal stress "$\sigma_{c,0D}$" is estimated in accordance with the auxiliary schematic in Fig. 1(a) and equation (1) which incorporates the stress concentration factor in accordance with reference [4].

$$\sigma_{c,0D} = K_t' \left(\frac{F_c}{A}\right) = K_t' \left(\frac{mR_{mean}\omega^2}{A}\right) = K_t' h \varrho R_{mean} \omega^2 \tag{1}$$

The stress concentration factor in equation (1) in dependency on the fraction of the fillet radius and the blade thickness is presented on the left-hand side of Fig. 2.

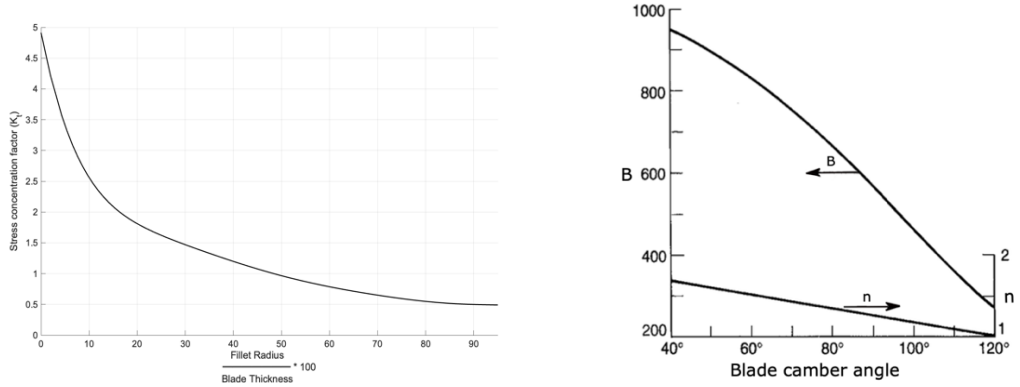


(a) (b)

Fig. 2 Supporting diagrams for the 0D analysis; (a) stress-concentration factor as a function of the fillet radius and the blade thickness (adopted from [4]), (b) section modulus determination diagram in accordance with Ainely(adopted [3])

## 2.2 Gas bending stresses

The force which produces a useful torque along with a gas bending moment in axial direction "$M_w$", emerges from a change in angular momentum of the gas in tangential direction. The maximum stresses can be calculated in accordance with bending theory. A turbine blade is sectioned into smaller strips of height, where the bending moment is calculated from the average force acting on each section. The gas bending stress is composed of the tensile stress – in the leading and trailing edges, and compressive stress – on the suction side of the blade. The highest value is typically observed at the leading or trailing edge of the root section [3], [12], [13]. Assuming the angle of incidence is zero at the design operating condition, the blade camber is virtually equal to the gas deflection, namely at the root. In dependency on the blade camber angle the values of "*n"* and "*B"* can be extracted from the diagram given in Fig. 2(b). Based on these values, the smallest value of the root section modulus ($\frac{I_{xx}}{y_{max}}$) of the turbine blade is calculated by:

$$z = \frac{I_{xx}}{y_{max}} = \frac{1}{B}\left(10\frac{t}{c}\right)^n c^3 \tag{2}$$

A useful approximation for preliminary design purposes is provided the following equation:

$$(\sigma_{gb})_{max,0D} \cong \frac{\dot{m}(C_{w2m}+C_{w3m})}{n\,\theta_{OTP}} \frac{h}{2}\frac{1}{z} \tag{3}$$

As for the considered partial admission turbine – the gas bending stress is reduced to zero in the non-admission parts of the turbine, the stress amplitude $\sigma_{a,0D}$ obtained by this 0D method is half of the max. gas bending stress:

$$\sigma_{a,0D} = \frac{\sigma_{gb,max,0D}}{2} \tag{4}$$

The mean stress $\sigma_{m,0D}$ obtained by this 0D method is the sum of the centrifugal stress and the stress amplitude:

$$\sigma_{m,0D} = \sigma_{c,0D} + \sigma_{a,0D} \tag{5}$$

DOI: 10.13009/EUCASS2022-6150



## 3. Structural 3D Finite Element Analysis Method

The turbine blade fatigue life method was evaluated with the use of the LUMEN LOx turbopump. Within the LUMEN LOx turbopump design, the bearings are lubricated by oil for improved life expectancy and modularity. Consequently, the replacement of the pump fluid by application of the oil-lubricated bearings for cooling, enables the research on independent systems, where turbine blade and pump components may be analysed without major turbopump redesigns [14]. A cross-section of the LOx turbopump is shown below in Fig. 3.

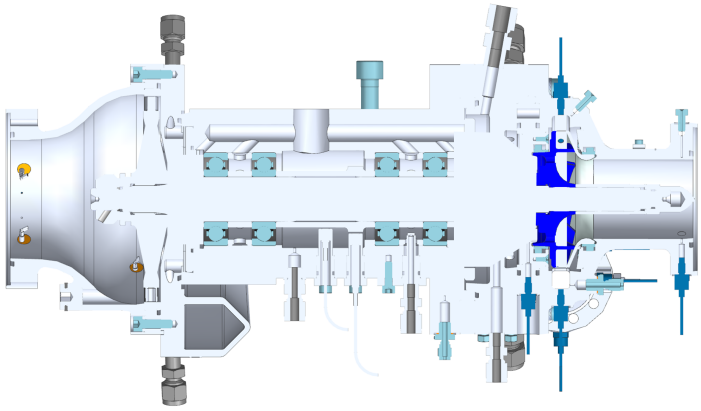

Fig. 3 LUMEN LOx turbopump cross-section (source: [14])

In the following subsections, the quasi-stationary structural 3D Finite Element LUMEN Oxygen turbopump analysis is presented. Within the developed model, the following load steps are applied:

- $LS_1$: Uniform thermal loading;
- $LS_2$: Additional spin loading (modelling centrifugal forces under elevated temperature and therefore, representing the loading of the turbine blade in the non-admission sections of the turbine);
- $LS_3$: Additional (circumferential) blade driving load in the admission sections of the turbine (caused by the turbine driving gas, emitted by the stator row).

The prime focus for the following post-processing HCF analysis is on $LS_2$ and $LS_3$, where the max. principal stresses at the highest loading point are evaluated.

### 3.1 Post-Processing HCF Life Analysis Method

Within the first step of the turbine blade HCF analysis, the maximum principal stresses of the highest loaded point of the turbine blade are extracted from load steps $LS_2$ and $LS_3$ of the structural 3D Finite Element analysis. Subsequently, the mean stress "$\sigma_{m,3D}$" (as mean value of the max. principal stresses of the two 3D Finite Element analysis load steps $LS_2$ and $LS_3$) and stress amplitude "$\sigma_{a,3D}$" (as half of the difference of the maximum principal stresses, extracted from the two considered 3D Finite Element analysis load steps $LS_3$ and $LS_2$) are calculated. As already described at the end of section 2 of this manuscript, the loads can alternatively be determined by applying a 0D analysis, based on the beam theory. Finally, the number of cycles to failure "$N_f$" is calculated by the following equation (as suggested in reference [15]):

$$N_f = \sqrt[B']{\frac{\sigma_a}{A'\left(1-\frac{\sigma_m}{C'}\right)}} \tag{6}$$

Contrary to the primary Goodman equation, with a stress amplitude "$\sigma_a$" being normalised by "$\sigma_{N_f}$" at fully reversed loading conditions "R=-1", "$\sigma_m = 0$" and the mean stress being normalised by the failure stress at constant loading conditions "R=1", "$\sigma_a = 0$" to the ultimate tensile stress; within the hereby presented modified Goodman equation (6), the "$\sigma_{N_f}$" is substituted by the stress amplitude "$\sigma_f$"at which the evaluated turbine blade material fails after "$N_f$" cycles at a given mean stress level ("$\sigma_m \neq 0$") and "$\sigma_{UTS}$" is replaced by a parameter C' [15].

DOI: 10.13009/EUCASS2022-6150



### 3.2 Structural 3D FEA – Loading and Boundary Conditions with Meshing and Material Parameters

The blade loading conditions of the LUMEN Oxygen turbine is evaluated for nine operating points, from which the structural-worst-case is established (recorded at the position of the blade leading edge). Accordingly with this data, the operating conditions with the highest amplitude and the smallest fatigue life is analysed, where loading conditions are highlighted in Table 2.

Table 2 Structural-worst-case operating point blade loading conditions of the LUMEN Oxygen TP

| ***Loading conditions*** | **Parameter** | **Value** | **Unit** |
|---|---|---|---|
| *Rotational speed OTP* | $\omega_{OTP,BP8}$ | 2806.5 | rad/sec |
| *Turbine driving gas temperature* | $T_{OTP,BP8}$ | 488.36 | K |
| *Single blade loading (in circumferential direction)* | $F_{single,BP8}$ | 49,37 | N |

The material used for the analysis of the LUMEN's Oxygen TP blade and disk is Inconel 718. For the sake of flexibility (e.g. follow-on Finite Element analysis of the remaining operating points of the LUMEN Oxygen TP blade), a temperature dependent modulus of elasticity (as shown on the left-hand side of Fig. 4) and a temperature dependent thermal expansion coefficient (as shown on the right-hand side of Fig. 4) are specified as input of the structural 3D Finite Element analysis.

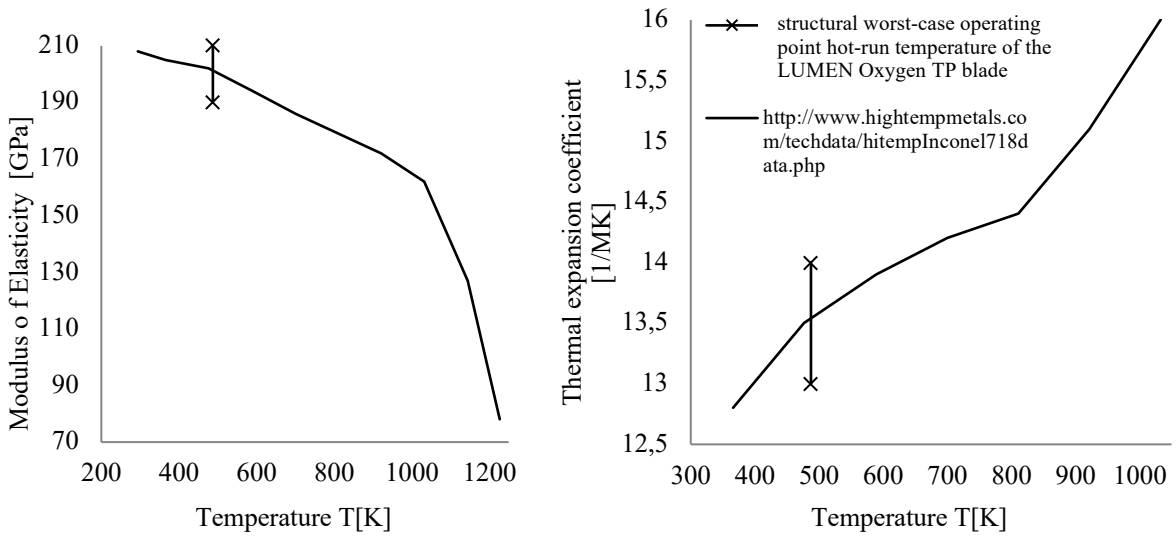


Fig. 4 Left: Temperature dependency of the modulus of elasticity; Right: thermal expansion coefficient of Inconel 718 at the structural worst-case hot-run operating point of the LUMEN Oxygen TP (M. T. Gulczyński *et al.*)

The HCF analysis parameters for Inconel 718, summarized in Table 3, are available for ambient temperature only (in accordance with reference [15]). The structural analysis parameters which are not temperature dependent, including density and Poisson's ratio, are equal to "$\varrho_{Inc718} = 8192[\frac{kg}{m^3}]$" and "ν=0.31" respectively.

Table 3 Parameters, used for the HCF analysis

| ***HCF analysis parameter*** | **Value** | **Unit** |
|---|---|---|
| $A'$ | 7160 | MPa |
| $B'$ | -0.1872 | - |
| $C'$ | 1154 | MPa |

On the left- hand side of Fig. 5, the structural boundary conditions applied to the 3D Finite Element model of the LUMEN Oxygen TP blade are presented. As may be observed in Fig. 5(a), the yellow faces represent symmetry boundary conditions applied. The blade driving force of "$F_{single}$ = 49.37 N", is distributed as a constant pressure on the surface highlighted with a red colour (always acting in the direction normal to the surface). The Finite Element mesh, used for the 3D analysis of the LUMEN Oxygen TP blade is shown in Fig. 5(b). The geometry is meshed with

DOI: 10.13009/EUCASS2022-6150



three different mesh sizes for increased accuracy. Gradual zoom levels – A(2:1) and B(3:1) – demonstrate the refinement of the Finite Element mesh in the vicinity of the maximum loading point of the model (the transition of the blade to the disk at the leading edge of the blade).

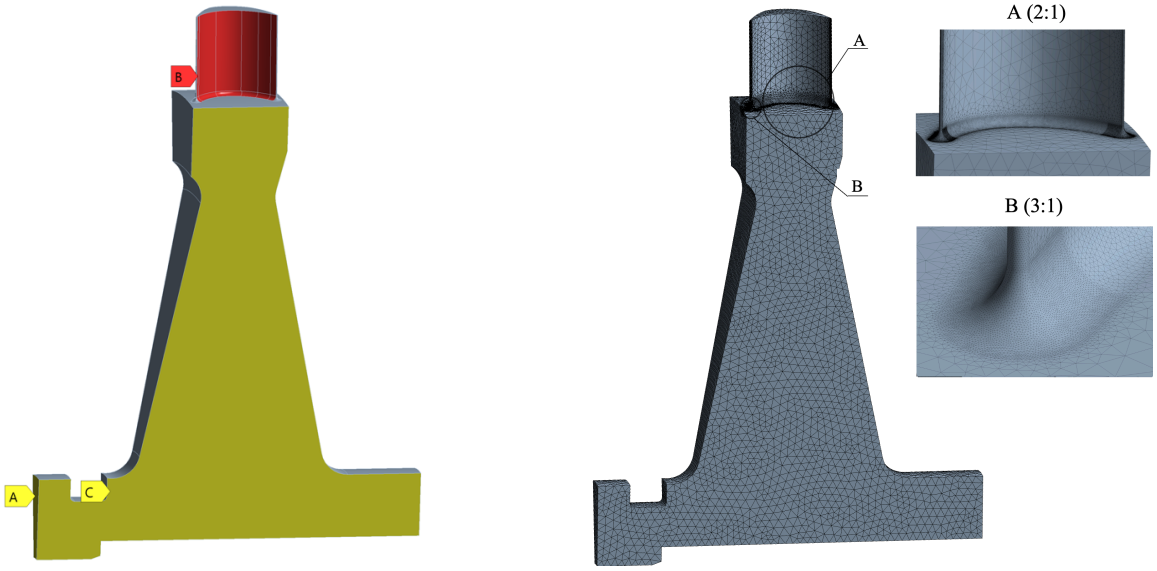


(a) (b)

Fig. 5 (a) Applied boundary conditions; (b) Finite Element Mesh as used for the structural 3D FEA of the LUMEN Oxygen TP blade and related disk section (M. T. Gulczyński *et al.*)

### 3.3 Structural 3D Finite Element Analysis Results

The maximum principal stress fields, obtained by load steps LS2 (combined thermal and centrifugal loading) and LS3 (combined thermal, centrifugal and gas bending loading) of the 3D FE analysis of the LUMEN Oxygen TP blade are presented in Fig. 6, respectively.

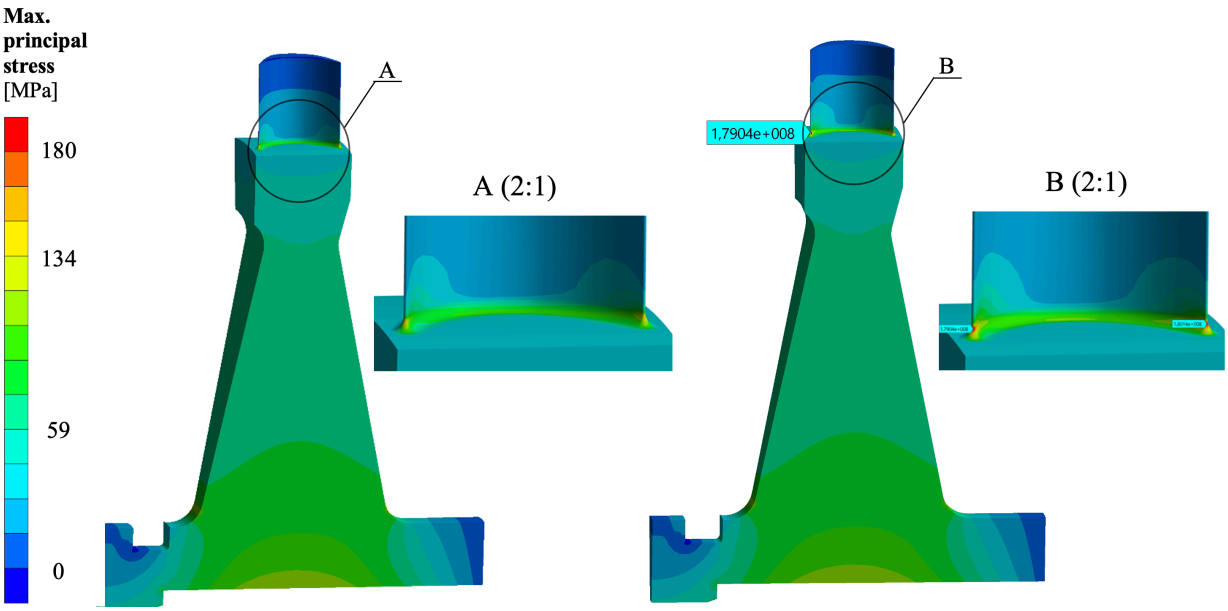


(a) (b)

Fig. 6 Max. principal stress fields, obtained by load steps $LS_2$ (a) and $LS_3$ (b) of the 3D Finite Element analysis of the LUMEN Oxygen TP blade (M. T. Gulczyński *et al.*)

DOI: 10.13009/EUCASS2022-6150



As it may be observed from the numerical analysis, for both cases $LS_2$ and $LS_3$, the max. principal stresses are recorded in the proximity of the turbine blade root on the pressure and the suction side of the blade. The stress is decreasing towards the tip – which is characteristic of the tensile load. The centrifugal stress is dependent on the blade material mass, blade length and the rotational speed. In Fig. 7 the max. principal stresses for transient loading in function of time recorded for 475 substeps is shown (left side), combined with a cross-section with max. principal stress fields for load step 2 ($LS_2$) and load step 3 ($LS_3$). As indicated, for the evaluated operating point, the max. principal stresses at the leading edge and trailing edge are of the similar values which is expected for a partial admission turbine.

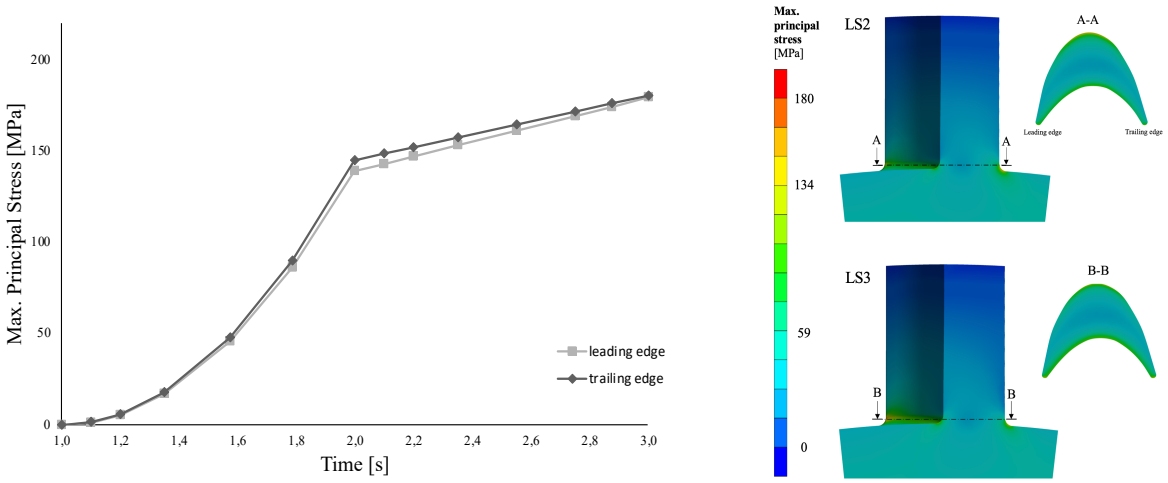


Fig. 7 Maximum Principal Stresses for the LUMEN LOx TP blade at leading and trailing edge for load step 2 – $LS_2$ and load step 3 – $LS_3$ (M. T. Gulczyński *et al.*)

For the numerical analysis, the min. principal stress is equal to "$\sigma_{c,3D} = 139[MPa]$" as obtained by the combination of centrifugal and thermal loading – $LS_2$. In case of combined thermal, centrifugal & max. gas bending loading – $LS_3$, the max. principal stress is equal to "$\sigma_{c,3D}+\sigma_{gb,max,3D} = 179[MPa]$". In comparison, within 0D analysis calculated with equations (1), (3), (4) and (5) and under equivalent loading conditions as well as with similar material parameters, the centrifugal and gas bending stress corresponds to "$\sigma_{c,0D} = 95.35[MPa]$" and "$\sigma_{gb,max,0D} = 29.80[MPa]$". The comparison of the numerical and analytical 0D results are summarized in Table 4.

Table 4 Results comparison obtained by 3D Finite Element and 0D beam theory analysis

| Nomenclature | Parameter | 3D FE analysis | 0D beam theory | Unit | 0D value / 3D value |
|---|---|---|---|---|---|
| Cyclic stress | $\sigma_{cyclic}$ | 40.4 | 29.80 | MPa | 27% |
| Stress amplitude | $\sigma_a$ | 20.2 | 14.9 | MPa | 27% |
| Mean stress | $\sigma_m$ | 158.9 | 125.15 | MPa | 21% |

The results obtained from the 0D beam theory were found to be approximately 25% smaller than the stresses received through the 3D Finite Element Analysis. This might be on account of stresses being calculated in radial direction of the turbine (equaling to the height direction of the turbine blade) for former, in contrast to max. principal stresses extracted for latter. Potential deviation could also be caused by the manual determination of the stress concentration factor "$K_t'$" together with "B" and "n" coefficients.

DOI: 10.13009/EUCASS2022-6150



### 3.4 Structural 3D Finite Element Analysis Results

The mean stress (green line) and the stress amplitude (violet line) as obtained by the 3D Finite Element analysis in relation to the test data given in Reference [15] (blue circles) used for fitting the HCF analysis parameters $A'$, $B'$ and $C'$ (as given in Table 3) is visualized in Fig. 8. The large gap between the (violet) stress amplitude line in Fig. 8 and the (blue) circles, indicates that the HCF analysis of the operating point of the considered turbine blade requires a large extrapolation of experimental HCF data. In order to visualize the HCF analysis according to equation (6), HCF life iso lines for 100 Mcycles, 10 Gcyles and 1 Tcycle were calculated by this equation and additionally included in Fig. 8 (combined with Haigh diagram for Inconel 718).

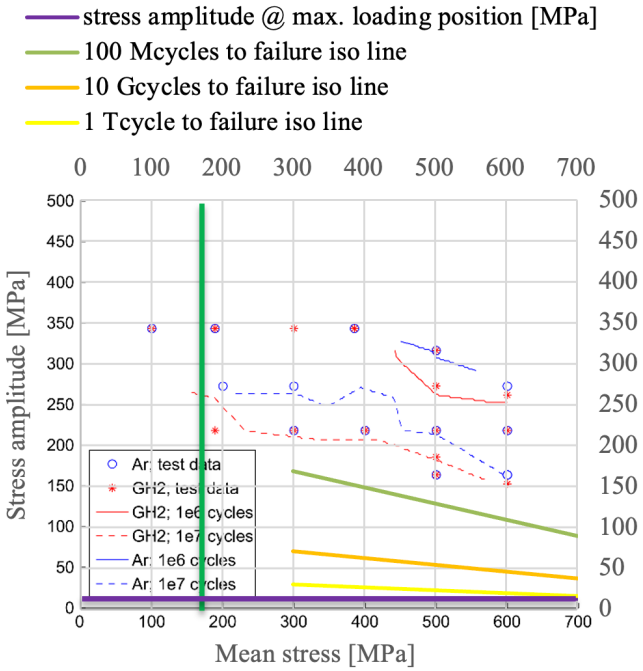


Fig. 8 Visualization of the structural-worst-case-operating point of the LUMEN Oxygen TP blade (crossing point of the green and the violet line) in relation to HCF test data (blue circles)

Due to the low stress amplitude of just 20 MPa, the HCF life of the LUMEN Oxygen TP blade, as predicted by equation (6), is as high as $N_f = 17$ trillion cycles before failure. On account of the effects highlighted below, which were only partially considered by the numerical analyses presented in this manuscript, the actual life of the turbine blades may result in lower number cycles before failure. To increase the performance and efficiency of the engine, a higher temperature in the turbomachinery component is inevitable. Therefore, it is especially important for the reusable engines that the turbomachinery components are evaluated to estimate the number of cycles to failure and evaluate fatigue behavior of the component especially w.r.t. the operating temperature. The evaluated turbopump material operates within the hot-run temperature range of approximately 500 K – where for Inconel 718 the yield strength within this temperature range is as high as "$\sigma_{\text{yield, Inconel718 at T=500 K}}$ =1100 MPa" [16]. Therefore, the life reduction due to thermal loading is found to have an insignificant influence. It is not excluded however, that lessening blade's life can be influenced by other effects, namely: multiaxial fatigue – combined high cycle fatigue (HCF) and low cycle fatigue (LCF) (as partly presented in reference [17]), creep or corrosion [18]. Further influence on the expected blade life might be related to free (damped) vibrations of the turbine (with the natural frequency of the turbine blades) in the non-admission sections of the turbine. A resonant interaction of the vibration of the turbine blade with other natural frequencies of the turbo pump (such as e.g. the rotor and the disk) during the start-up and shut-down phases of the turbo pump operation, could reduce the life of the blades. This is of particular importance when considering the reusability applications of the engine.

DOI: 10.13009/EUCASS2022-6150



## 4. Summary and Outlook

Within the presented manuscript, two structural analysis methods were compared: A 0D analysis – based on the beam theory, and a 3D Finite Element method. Both of the HCF life relevant structural analysis results (mean stress and stress amplitude), obtained by applying the 0D beam theory to a blade of the LUMEN Oxygen TP were found to be within an acceptable margin with the respective results, obtained by the 3D FE analysis. The post-processing HCF analysis, based on the max. principal stress values of the above-mentioned 3D Finite Element analysis, resulted in a fatigue life of 17 trillion cycles before failure. The foreseen improvements of the presented methods will include a mesh convergency study along with a transient analysis of the damped vibration of the turbine blade in the non-admission sections of the turbine. Furthermore, an extended fatigue life analysis with components of the turbine driving load acting in axial direction of the turbine blade will be assessed. For the post-processing HCF evaluation, additional tests are foreseen with an improved operating conditions representation - what should result in an enhanced validation model. Furthermore, the study of the turbopump life reduction due to elevated temperatures is envisioned, which shall ensure the versatility of the hereby presented methods when evaluating turbopumps working in wider spectrum conditions, e.g. LUMEN's fuel turbopump operating within higher temperature range.

## Acknowledgement

The project leading to this manuscript has received funding from the European Union's Horizon 2020 research & innovation programme under the Marie Skłodowska-Curie grant agreement No 860956.

## References

[1] T. Traudt, G. Waxenegger-Wilfing, R. D. S. Hahn, B. Wagner, and J. Deeken, "An overview on the turbopump roadmap for the LUMEN demonstrator engine and on the new turbine test facility," *Proc. Int. Astronaut. Congr. IAC*, vol. 13, no. September, pp. 8513–8517, 2017.

[2] S. C. S. Chen, J. P. Veres, and J. E. Fittje, "Turbopump design and analysis approach for nuclear thermal rockets," *AIP Conf. Proc.*, vol. 813, no. January 2006, pp. 522–530, 2006, doi: 10.1063/1.2169230.

[3] H. I. H. Saravanamuttoo, H. Cohen, G. F. C. Rogers, P. V. Straznicky, and A. C. Nix, *Gas Turbine Theory SEVENTH EDITION Gas Turbine Theory*. 2017.

[4] N. A. and S. Administration, "NASA SP-8110 Liquid Rocket Engine Turbines," 1974.

[5] G. P. Sutton and O. Biblarz, *Rocket Propulsion Elements*, Ninth Edit. John Wiley & Sons, 2016.

[6] M. T. Gulczynski *et al.*, "RLV applications: challenges and benefits of novel technologies for sustainable main stages," Oct. 2021. [Online]. Available: https://elib.dlr.de/148758/

[7] M. T. Gulczyński, J. R. Riccius, G. Waxenegger-wilfing, J. C. Deeken, and M. Oschwald, "Numerical Fatigue Life Analysis of Combustion Chamber Walls for Future Reusable Liquid Rocket Engines (LREs) Applications," 2022, no. SP2022, pp. 1–14.

[8] R. H. S. Hahn, M. T. Gulczyński, E. Kurudzija, K. Dresia, G. Waxenegger-Wilfing, and J. Deeken, "LUMEN EVOLUTION FOR LUNAR LANDER PROPULSION," 2022.

[9] Robson H. S. Hahn, Jan C. Deeken, Tobias Traudt, Michael Oschwald, Stefan Schlechtriem, and Hideyo Negishi, "LUMEN Turbopump -Preliminary CFD Analysis of a Supersonic Turbine," pp. 9–10, 2019.

[10] Z. Dżygadło, M. Łyżwiński, J. Otyś, S. Szceciński, and R. Wiatrek, *Napędy Lotnicze - Zespoły Wirnikowe Silników Turbinowych*. Wydawnictwo Komunikacji i Łączności, 1982.

[11] W. Zhang, *Failure characteristics analysis and fault diagnosis for liquid rocket engines*. 2016.

[12] Г. Г. Гахун and . и др (сост.), *КОНСТРУКЦИЯ И ПРОЕКТИРОВАНИЕ ЖИДКОСТНЫХ РАКЕТНЫХ ДВИГАТЕЛЕЙ*. Москва Машиностроение, 1989.

[13] J. R. Riccius, E. B. Zametaev, M. T. Gulczyński, and R. H. S. Hahn, "NUMERICAL LRE TURBINE BLADE FATIGUE LIFE ANALYSIS TAKING INTO ACCOUNT PARTIAL ADMISSION EFFECTS," 2022.

[14] T. Traudt, R. H. S. Hahn, T. Mason, J. C. Deeken, M. Oschwald, and S. Schlechtriem, "LUMEN Turbopump - Design and Manufacturing of the LUMEN LOX and LNG Turbopump components," 2019.

[15] M. Bruchhausen, B. Fischer, A. Ruiz, S. González, P. Hähner, and S. Soller, "Impact of hydrogen on the high cycle fatigue behaviour of Inconel 718 in asymmetric push-pull mode at room temperature," *Int. J. Fatigue*, vol. 70, pp. 137–145, 2015, doi: 10.1016/j.ijfatigue.2014.09.005.

[16] Y. Zhang *et al.*, "Microstructures and properties of high-entropy alloys," *Prog. Mater. Sci.*, vol. 61, no. November 2013, pp. 1–93, 2014, doi: 10.1016/j.pmatsci.2013.10.001.

[17] J. R. Riccius, E. B. Zametaev, and L. J. Souverein, "HCF, LCF and creep life analysis of a generic LRE turbine blade," *AIAA Sci. Technol. Forum Expo. AIAA SciTech Forum 2022*, 2022, doi: 10.2514/6.2022-0796.

[18] S. P. Zhu, P. Yue, Z. Y. Yu, and Q. Wang, "A combined high and low cycle fatigue model for life prediction of turbine blades," *Materials (Basel).*, vol. 10, no. 7, pp. 1–15, 2017, doi: 10.3390/ma10070698.